JBC RESEARCH ARTICLE

TMEM2 inhibits the development of Graves' orbitopathy through the JAK-STAT signaling pathway

Received for publication, May 11, 2023, and in revised form, November 13, 2023 Published, Papers in Press, December 28, 2023,
https://doi.org/10.1016/j.jbc.2023.105607

Hong Li[*,‡], **Jie Min**[‡], **Yucheng Yang, Wendong Suo, Wei Wang, Jiahe Tian, and Yujie Qin**
From the Department of Endocrinology, LongHua Hospital Shanghai University of Traditional Chinese Medicine, Shanghai, China

Reviewed by members of the JBC Editorial Board. Edited by Clare E. Bryant

A mouse model was used to investigate the role of the hyaluronidase, transmembrane protein 2 (TMEM2), on the progression of Graves' orbital (GO) disease. We established a GO mouse model through immunization with a plasmid expressing the thyroid stimulating hormone receptor. Orbital fibroblasts (OFs) were subsequently isolated from both GO and non-GO mice for comprehensive *in vitro* analyses. The expression of TMEM2 was assessed using qRT-PCR, Western blot and immunohistochemistry *in vivo*. Disease pathology was evaluated by H&E staining and Masson's trichrome staining in GO mouse tissues. Our investigation revealed a notable reduction in TMEM2 expression in GO mouse orbital tissues. Through overexpression and knockdown assays, we demonstrated that TMEM2 suppresses inflammatory cytokines and reactive oxygen species production. TMEM2 also inhibits the formation of lipid droplets in OFs and the expression of adipogenic factors. Further incorporating Gene Set Enrichment Analysis of relevant GEO datasets and subsequent *in vitro* cell experiments, robustly confirmed that TMEM2 overexpression was associated with a pronounced upregulation of the JAK/STAT signaling pathway. *In vivo*, TMEM2 overexpression reduced inflammatory cell infiltration, adipogenesis, and fibrosis in orbital tissues. These findings highlight the varied regulatory role of TMEM2 in GO pathogenesis. Our study reveals that TMEM2 plays a crucial role in mitigating inflammation, suppressing adipogenesis, and reducing fibrosis in GO. TMEM2 has potential as a therapeutic target and biomarker for treating or alleviating GO. These findings advance our understanding of GO pathophysiology and provide opportunities for targeted interventions to modulate TMEM2 for therapeutic purposes.

Graves' orbitopathy (GO), also named Graves' orbitopathy, thyroid-associated ophthalmopathy, or thyroid eye disease, is the most common complication of Graves' disease, an autoimmune disorder that negatively impacts the quality of life of patients by impairing visual function and causing cosmetic disfigurement (1). GO is characterized by inflammation, expansion, remodeling and fibrosis of the orbital tissue, and orbital fibroblasts (OFs) have been shown to be key target and effector cells that contribute to its pathogenesis (2). During GO progression, immune cells infiltrate the orbital tissue leading to activation of OFs. Activated OFs then secrete inflammatory mediators such as chemokines and cytokines that act on immune cells to amplify the immune response. This leads to expression of extracellular matrix proteins by OFs, and OF proliferation and differentiation into myofibroblasts or adipocytes, which contribute to fibrosis, expansion and remodeling of the orbital tissue (3, 4). A better understanding of the mechanisms leading to inflammation, adipogenesis and fibrosis in GO would be beneficial for the development of novel treatment strategies.

Hyaluronic acid (HA) is an extracellular matrix glycosaminoglycan that has been shown to mediate multiple cellular processes including cell-cell and cell-matrix adhesion, cell-cell signaling, migration of immune cells, and proliferation (5, 6). HA is overproduced by OFs in GO and has been implicated in the pathogenesis of this disease (7, 8). Due to its hydrophilic nature, HA binds to large amounts of water, thereby contributing to the edema of orbital tissues and subsequent protrusion of the eye (9). A role for HA and hyaluronidases in mediating adipogenesis has also been described (10). Thus, many studies have focused on targeting HA as a potential therapeutic strategy for GO either by inhibiting its synthesis or promoting its degradation.

Degradation of HA is mediated by the HYAL family of hyaluronidases, which includes HYAL1, HYAL2, HYAL3, HYAL4, and PH-20/SPAM1 (11, 12) as well as the more recently identified Transmembrane two protein (TMEM2) (13). Recently, HYAL1 was found to inhibit reactive adipogenesis and inflammation in the colon and skin, indicating that targeting HA catabolism could be beneficial therapeutically (10). TMEM2 plays a key role in mediating contact-dependent degradation of HA, and is also a key regulator of integrin-mediated cell-substrate adhesion (13, 14). Thus, targeting HA degradation is potentially a viable therapeutic strategy to treat GO.

TMEM2 is a member of the interferon-induced transmembrane protein superfamily and has also recently been identified as the only transmembrane hyaluronidase (15). TMEM2 has been associated with a wide range of conditions including bladder, breast and pancreatic cancer (16–18), and endoplasmic reticulum stress (19). TMEM2 has also been shown to have antiviral activity by activating the Janus kinase (JAK)/signal transducer and activator of transcription (STAT)

‡ These authors contributed equally to this work.
* For correspondence: Hong Li, lh2418@shutcm.edu.cn.

© 2023 THE AUTHORS. Published by Elsevier Inc on behalf of American Society for Biochemistry and Molecular Biology. This is an open access article under the CC BY-NC-ND license (http://creativecommons.org/licenses/by-nc-nd/4.0/).

signaling pathway that is a master regulator of several other downstream signaling pathways (20). However, despite the importance of OFs and HA in GO, the role of TMEM2 in GO has not been examined.

In this study, we identify a role for TMEM2 in a mouse model of GO. TMEM2 expression is reduced in GO tissues, while overexpression of TMEM2 reduces inflammation, adipogenesis, and fibrosis. TMEM2 acts *via* the JAK/STAT pathway to reduce the severity of GO, identifying TMEM2 as a potential therapeutic target to treat GO.

Results

TMEM2 expression levels are decreased in a mouse model of GO

To determine the role of TMEM2 in GO, we developed a mouse model of GO (Fig. 1*A*) by immunizing mice with a plasmid encoding TSHR A as previously described (21). Consistent with the immunological aspects of GO, we assessed CD3 expression as a marker for T lymphocytes (22), highlighting the involvement of T lymphocytes in the immune response within the orbital tissues (Fig. 1*B*). We found that TMEM2 protein and mRNA expression levels were significantly decreased in GO tissue samples compared to non-GO tissue samples by Western blot and qRT-PCR analysis, respectively (Fig. 1, *C* and *D*). Similarly, IHC staining of mouse GO and non-GO tissue samples revealed decreased TMEM2 expression levels in GO tissues (Fig. 1*E*). Together, these results suggest that decreased TMEM2 expression is associated with GO.

TMEM2 inhibits ROS production in OFs and alleviates inflammation

We next performed gain-of-function and loss-of-function assays in OFs derived from non-GO tissues to determine the role of TMEM2 in GO. First, we established that our TMEM2 overexpression and shTMEM2 vectors successfully increased or reduced TMEM2 protein expression levels (Fig. 2*A*). We then examined if TMEM2 affected the inflammatory response in OFs. We treated cells with H_2O_2 to induce ROS production and found that overexpression of TMEM2 inhibited ROS production in both untreated and H_2O_2-treated cells, whereas knockdown of TMEM2 had no effect (Fig. 2*B*). Cells were then treated with IL-1β to induce an inflammatory response, which was assessed by measuring the relative expression levels of IL-6 and IL-8 by ELISA. We found that overexpression of TMEM2 significantly reduced IL-6 and IL-8 levels in IL-1β-treated cells, whereas knockdown of TMEM2 interestingly had no effect (Fig. 2*C*). We then examined how the expression of TMEM2 was affected by inflammatory response in OFs. We found that knockdown of TMEM2 cannot break through the low expression caused by inflammatory response (Fig. 2, *D* and *E*). Together, our findings suggest that overexpression of TMEM2 inhibits ROS production and reduces inflammatory cytokine production in OFs.

TMEM2 inhibits the adipogenic differentiation of orbital fibroblasts

Since OFs have been reported to differentiate into adipocytes in response to inflammatory cytokines (21, 23), we next

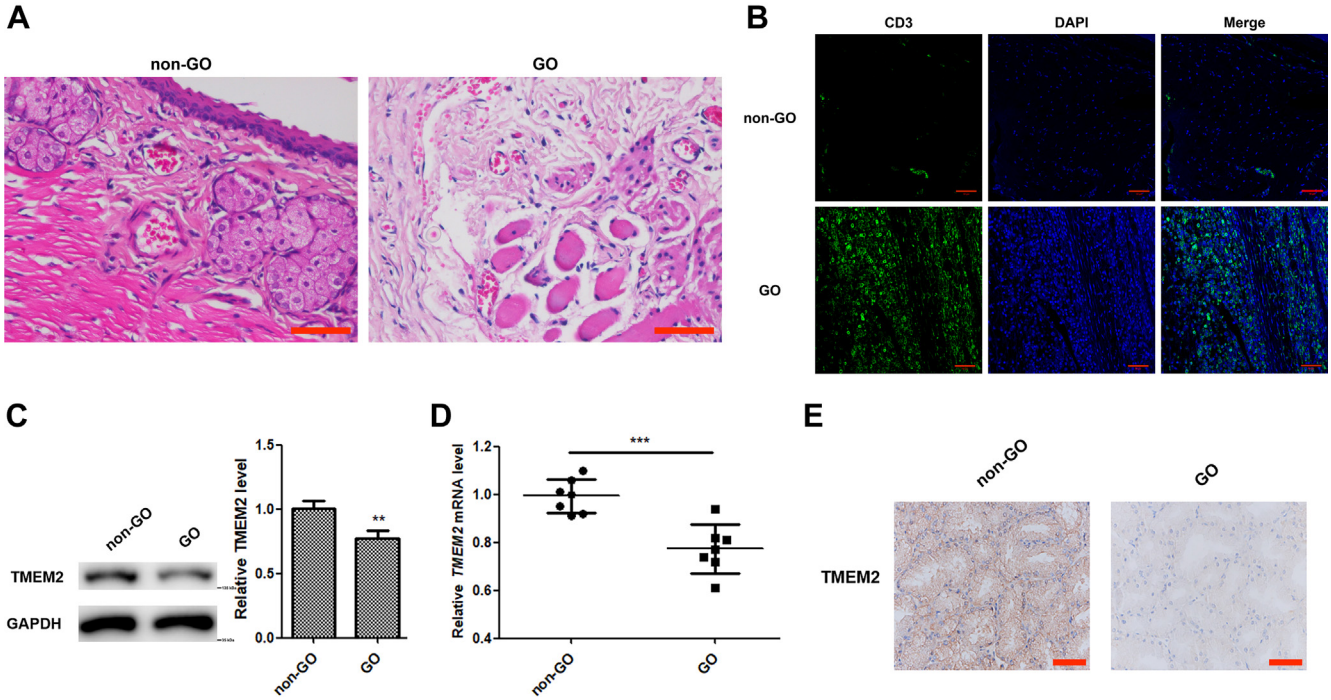

Figure 1. A mouse model of GO was constructed. TMEM2 expression levels are decreased in GO. *A*, representative images of pathological tissue of GO mouse models detected by H&E (×400), n = 5, scale bar = 50 μm. *B*, representative images of $CD3^+$ T cells at pathological sites detected by immunofluorescence, n = 5, scale bar = 50 μm. *C*, TMEM2 protein expression levels were detected in GO and non-GO tissues by western blotting, n = 5. *D*, qPCR was used to detect *TMEM2* mRNA levels in GO and non-GO tissues, n = 7. *E*, representative IHC images showing TMEM2 protein expression in GO and non-GO tissues, n = 5, scale bar = 50 μm. Data are presented as mean ± SD, $^{***}p < 0.001$.

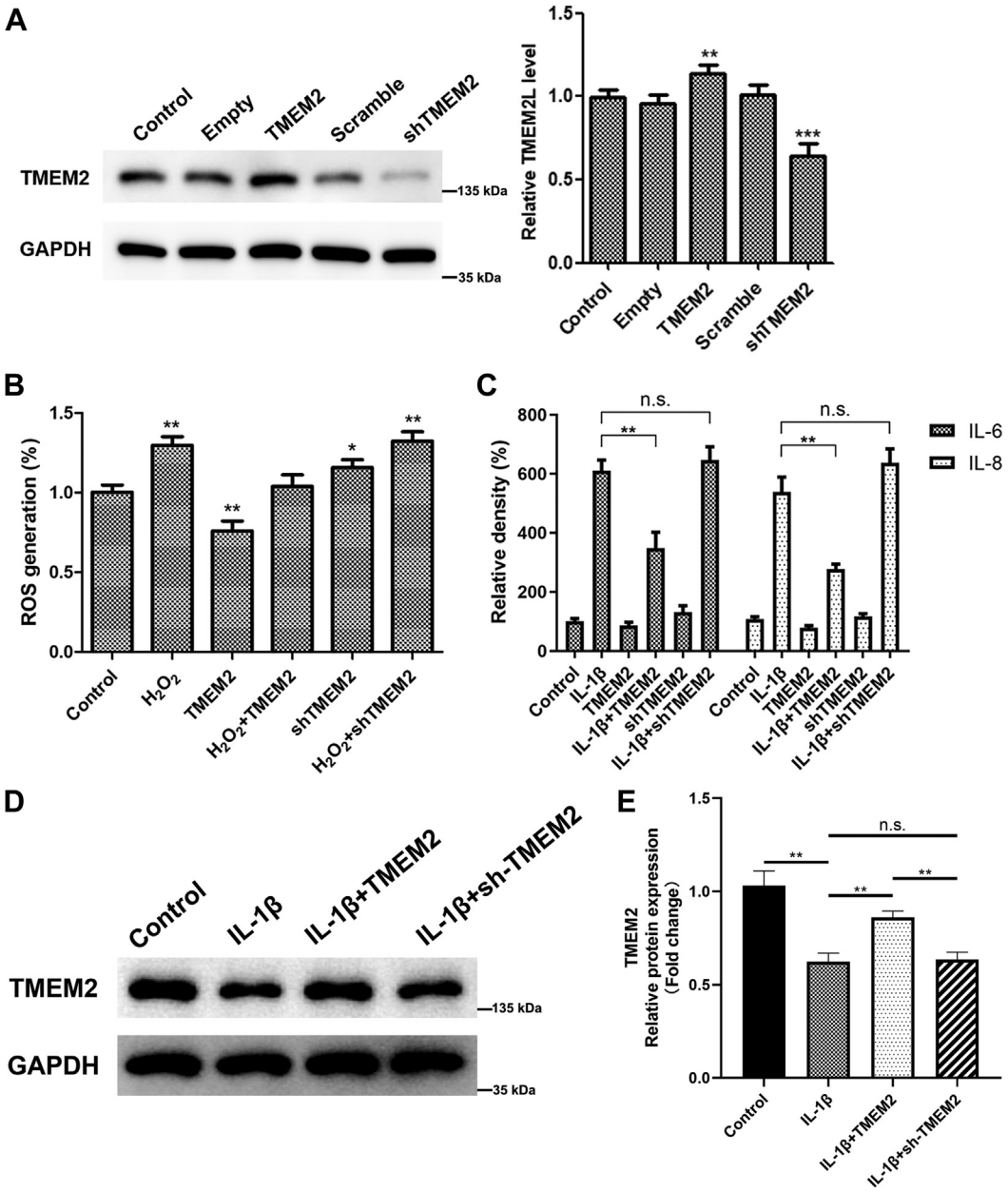

Figure 2. TMEM2 inhibits ROS production in orbital fibroblasts and alleviates inflammation. *A*, Western blotting was used to detect TMEM2 protein expression levels in cells after overexpression/knockdown, n = 3. *B*, OFs were treated with H_2O_2 to induce ROS production. The effects of TMEM2 overexpression and knockdown on ROS production were examined in H_2O_2-treated OFs, n = 3. *C*, OFs were treated with IL-1β to induce an inflammatory response. The effects of TMEM2 overexpression and knockdown on the IL-1β-induced inflammatory response were examined by measuring the relative expression levels of IL-6 and IL-8 by ELISA, n = 5. *D* and *E*, TMEM2 protein expression levels were detected in OFs by western blotting after being treated with IL-1β, n = 3. Data are presented as mean ± SD. ns, no significance, *$p < 0.05$, ** represents $p < 0.01$, *** represents $p < 0.001$.

sought to determine the role of TMEM2 in adipogenic differentiation. We induced adipogenic differentiation in OFs and oil red O staining revealed that overexpression of TMEM2 significantly reduced the frequency of lipid droplets compared to control cells, whereas knockdown of TMEM2 led to a significant increase (Fig. 3, *A*, *C*, and *D*). We also examined the expression levels of key proteins involved in promoting adipogenesis including PPAR-γ and c/EBP-α and adiponectin, which is the most abundant peptide secreted by adipocytes (24). Consistent with the oil red O staining, we found that adiponectin, PPAR-γ and c/EBP-α protein expression levels were significantly reduced following TMEM2 overexpression, while TMEM2 knockdown led to increased expression (Fig. 3*B*). c/EBP-β expression levels were unaffected. Together, these findings suggest that overexpression of TMEM2 inhibits adipogenic differentiation in OFs.

TMEM2 functions through the JAK-STAT signaling pathway

Since TMEM2 has been shown to activate JAK/STAT signaling (20) and the JAK/STAT signaling pathway has been implicated in mediating the disease progression of many

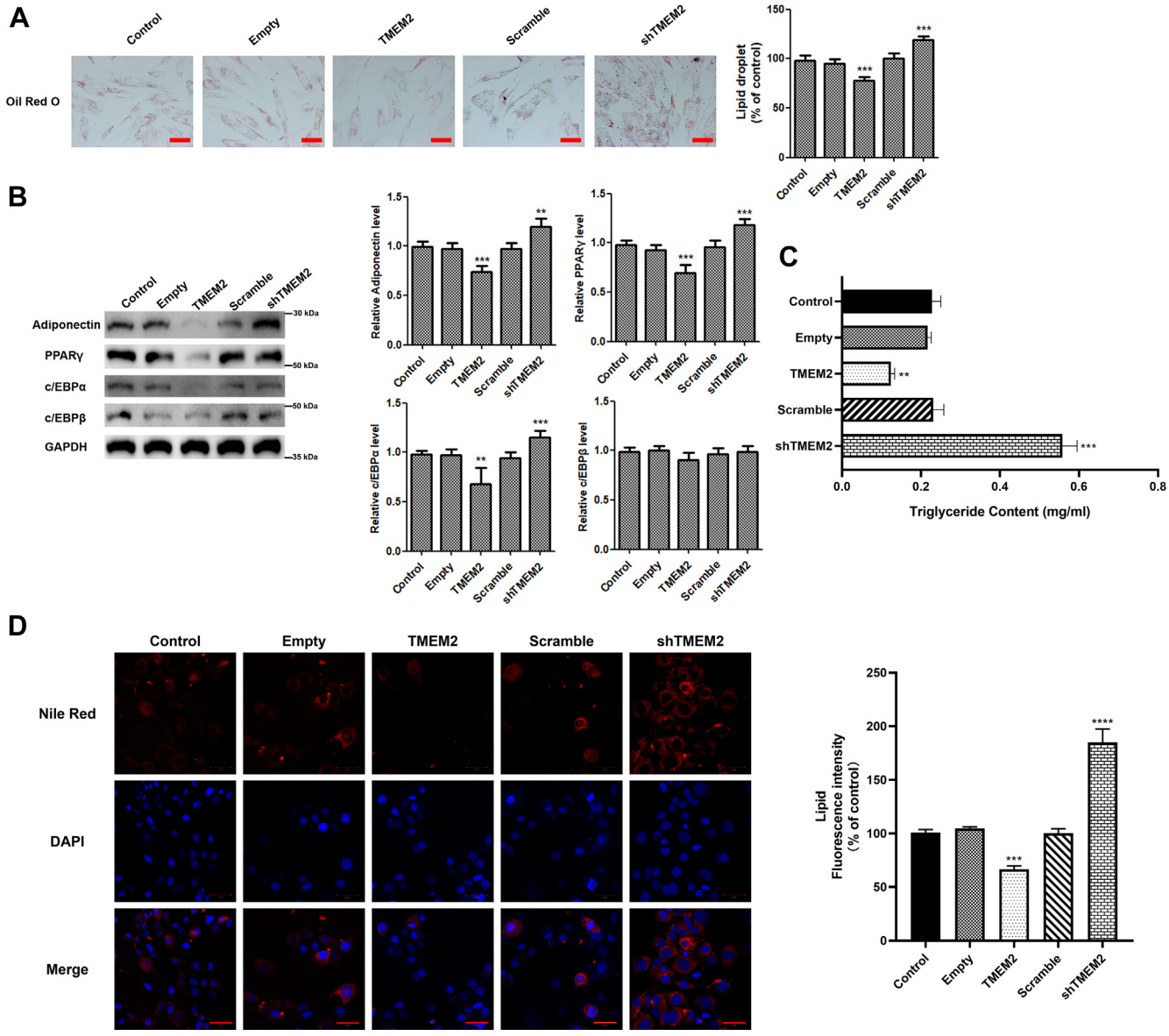

Figure 3. TMEM2 inhibits the adipogenic differentiation of orbital fibroblasts. *A*, the effects of TMEM2 overexpression and knockdown on cell lipid droplet generation were examined by oil red O staining, n = 3, scale bar = 50 μm. *B*, Western blot analysis was used to examine the protein expression levels of adipogenic-associated proteins including adiponectin, PPAR-γ, c/EBP-α and c/EBP-β, n = 3. *C*, triglyceride expression levels were examined by ELISA, n = 5. *D*, lipid droplets level in OFs was examined by Nile Red staining, n = 3, scale bar = 50 μm. Data are presented as mean ± SD. $^{**}p < 0.01$, $^{***}p < 0.001$.

autoimmune and inflammatory diseases, we next examined if TMEM2 activated the JAK/STAT pathway in OFs. In the validation set GSE116959 from the GEO dataset, samples of OFs stimulated with or without TGF-β1 from patients with GO were divided into low and high groups according to the expression level of the genes. Gene set enrichment analysis (GSEA) was conducted and mapped into the KEGG pathway enrichment database. The terms with p-value < 0.05 were chosen as the cutoff criteria. Upon conducting GSEA analysis, we observed a positive correlation between the expression of TMEM2 and the JAK/STAT signaling pathway. This suggests a potential positive regulatory relationship between the two (Fig. 4*A*). As shown in Figure 4, *B–E*, overexpression of TMEM2 led to increased phosphorylation of Tyk2, JAK1, Stat1, and Stat2, without affecting levels of the non-phosphorylated forms of these proteins. Further, we next treated OFs with CYT387 (5 μM), a Jak1 inhibitor (25). Inhibition of Jak1 phosphorylation reversed the increase in downstream STAT pathway phosphorylation caused by overexpression of TMEM2 (Fig. 4, *G–J*), as well as the frequency of lipid droplets (Fig. 4, *K* and *L*), which leads to a specific signaling pathway of TMEM2-JAK/STAT axis. Thus, these results suggest that the effects of TMEM2 in OFs are dependent upon increased JAK/STAT signaling.

TMEM2 inhibits the progression of Graves' orbital disease in vivo

Finally, the effects of TMEM2 overexpression on the progression of Graves' orbital disease were examined in our

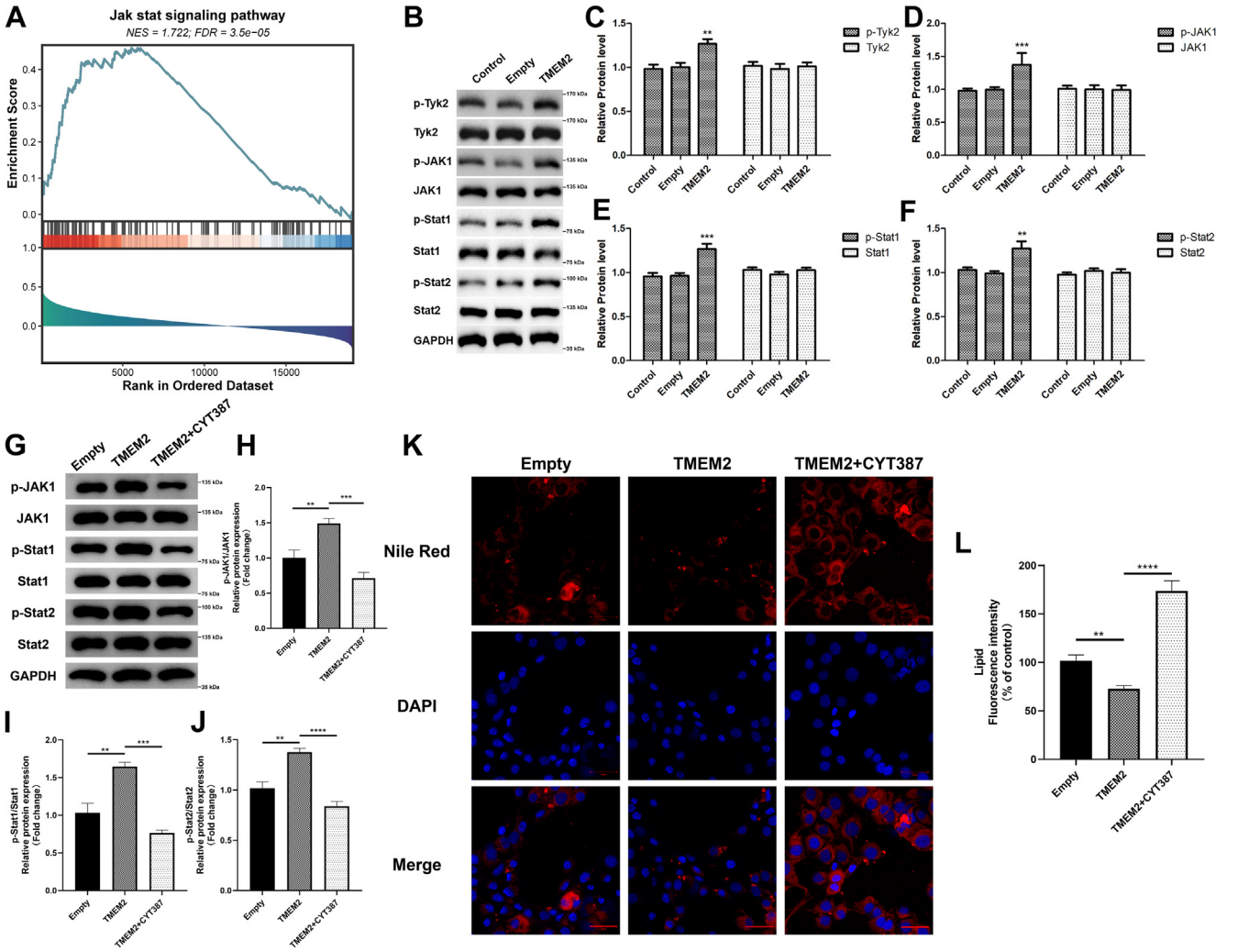

Figure 4. TMEM2 activates the JAK-STAT signaling pathway *in vitro*. *A*, TMEM2-induced changes in gene expression were analyzed by GSEA. *B–F*, protein expression and phosphorylation levels of components of the JAK-STAT signaling pathway were detected by western blotting. *G–J*, OFs were treated with CYT387 (5 μM) to inhibit JAK1 phosphorylation. The expressions of downstream Stat1 and Stat2 phosphorylation were examined by western blotting. *K* and *L*, relevant lipid droplets level in OFs was examined by Nile Red staining, scale bar = 50 μm. Data are presented as mean ± SD, n = 3, $^{**}p < 0.01$, $^{***}p < 0.001$, $^{****}p < 0.0001$.

mouse model of GO. We observed lymphocytic infiltrate into the orbital tissues and strikingly, overexpression of TMEM2 significantly reduced the inflammatory infiltration (Fig. 5*A*). Further, the increased adipogenesis observed in mouse GO tissue was significantly reduced following overexpression of TMEM2 (Fig. 5, *B*, *D–F*). TMEM2 overexpression was also associated with reduced fibrosis as measured by Masson's trichrome staining (Fig. 5*C*). Overexpression of TMEM2 also reversed GO induced T cell activation and inhibited cellular immune response (Fig. 5, *G* and *H*). Taken together, these findings demonstrate that overexpression of TMEM2 reduced disease progression in a mouse model of GO.

Discussion

GO is an autoimmune disease that is characterized by the inflammation, expansion, remodeling and fibrosis of the orbital tissue (2, 26). Elevated levels of several proteins, including human TSH receptor (hTSHR) and HA mediate fibrosis of orbital muscle tissue and tissue edema that potentiates inflammatory cell infiltration, respectively (27, 28). Multiple studies have suggested that targeting HA could be potentially beneficial in the development of novel therapeutic strategies for GO (29). For example, two independent studies recently demonstrated that 4-methylumbelliferone could inhibit HA synthesis and adipogenesis in cultured OFs (8, 30), while Zhang *et al* demonstrated that combined inhibition of PI3K1A and mTORC1 decreased HA production and adipogenesis (31). However, targeting HA catabolism to treat GO has not been examined. In the current study, we focused on the role of HA degradation in GO disease progression. Specifically, we found that the hyaluronidase TMEM2 was significantly downregulated in orbital tissue isolated from GO-induced mice, while overexpression of TMEM2 protected mice from the development of disease in a model of GO. Thus, we show for the first time that reduced expression of TMEM2 could account for increased HA levels and adipogenesis associated with GO, and that TMEM2 is a potential therapeutic target in GO.

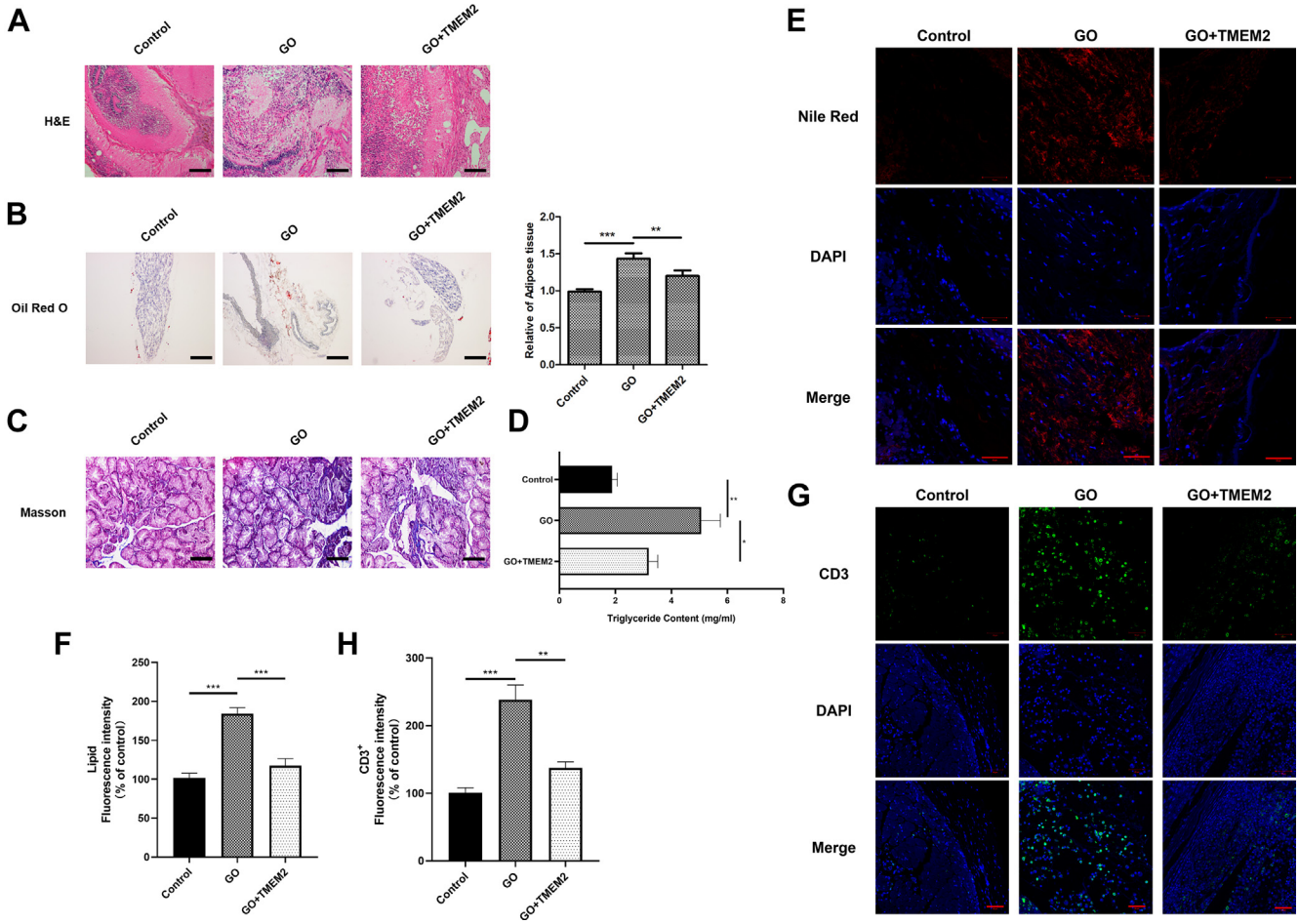

Figure 5. TMEM2 inhibits the progression of Graves' orbital disease *in vivo*. *A*, representative images of pathological tissue of GO mouse models detected by H&E (×40), scale bar = 50 μm, n = 5. *B*, representative images of adipose tissue at pathological sites were detected by oil red O staining, scale bar = 50 μm, n = 5. *C*, representative images of fibrous formation at pathological sites detected by Masson's trichrome staining, scale bar = 50 μm, n = 5. *D*, triglyceride expression levels of pathological tissue were examined by ELISA, n = 7. *E* and *F*, lipid droplets level of pathological tissue was examined by Nile Red staining, scale bar = 50 μm, n = 5. *G* and *H*, representative images of $CD3^+$ T cells at pathological sites detected by immunofluorescence, n = 5, scale bar = 50 μm. Data are presented as mean ± SD. $^{**}p < 0.01$, $^{***}p < 0.001$.

Since both ROS and IL-1β have key roles in mediating the progression of inflammatory disorders (32, 33), we next examined the effects of TMEM2 overexpression and knockdown on H_2O_2- and IL-1β-treated OFs. We found that overexpression of TMEM2 inhibited ROS production and alleviated inflammation in OFs. Furthermore, we found that overexpression of TMEM2 inhibited adipogenic differentiation of OFs, which occurs in response to inflammatory cytokines (21, 23).

Additionally, the fact that TMEM2 overexpression exerted notable effects on key cellular processes, despite a less-than-expected increase in expression levels, suggests a complex interplay of factors governing its functionality. The observed functional consequences emphasize the significance of even subtle shifts in protein levels. It is plausible that TMEM2, like many regulatory proteins, operates within a finely tuned range where small variations trigger significant cellular responses. This echoes the concept that biological systems often exhibit non-linear relationships between protein expression and functional outcomes. Our findings, therefore, contribute to the growing understanding that the impact of protein modulation extends beyond a simple dose-response paradigm. Conversely, the observed 20% downregulation of TMEM2 in the GO mouse model adds another layer of complexity to our understanding. While seemingly modest, this reduction may carry functional significance within the specific context of GO. The dynamic and multifaceted nature of GO, characterized by immune responses, inflammation, and tissue remodeling, could contribute to the observed regulatory changes. The seemingly modest changes in TMEM2 expression levels, both in overexpression and downregulation scenarios, highlight the need for a more comprehensive understanding of the intricate molecular mechanisms governing TMEM2's functionality in the context of GO.

The signaling pathways by which TMEM2 mediates its effects are not well known. Recently, TMEM2 was shown to inhibit HBV infection in HCC cells *via* activation of the JAK/STAT signaling pathway (20, 34). Since the JAK/STAT signaling pathway has also been implicated in mediating the disease progression of many autoimmune and inflammatory diseases, we sought to determine whether TMEM2 reduced adipogenesis of OFs through JAK/STAT signaling. Western

blot analysis revealed that overexpression of TMEM2 led to increased phosphorylation of Tyk2, JAK1, Stat1, and Stat2. Thus, therapies resulting in enhanced JAK/STAT signaling may be beneficial in GO. Consistent with this, inhibition of the JAK2/TYK2 phosphatase PTP1B in GO has been shown to reduce inflammation, ROS generation, and fibrosis (35), which is similar to the effects of TMEM2 overexpression. Thus, TMEM2-dependent modulation of JAK/STAT signaling may provide a novel therapeutic modality to treat GO.

TMEM2 expression is regulated by SOX4, a gene located in the 6p region that has been previously associated with Graves' disease in a genome-wide association study (36). Thus, reduced TMEM2 expression in GO may also be associated with dysfunctional SOX4. The SOX4/TMEM2 axis in GO will be the subject of future studies.

In conclusion, our study defined a role for TMEM2 in the regulation of inflammation, adipogenesis, and fibrosis associated with GO disease progression. We found that TMEM2 activates the JAK/STAT pathway to reduce the severity of GO and identifies TMEM2 as a potential therapeutic target to treat GO.

Experimental procedures

Construction of a mouse model of Graves' orbital disease

Female BALB/c mice aged 6 to 8 weeks were purchased from Liaoning Changsheng Biotechnology Ltd. Mice were housed under specific pathogen-free conditions and given free access to food and water. All animal experiments were approved by the Animal Research Ethics Committee of Longhua Hospital. We established the *in vivo* GO mouse model as described previously (21). Briefly, mice were anesthetized by intraperitoneal injection of sodium pentobarbital (40 mg/kg), then injected intramuscularly (in the biceps femoris muscle) with plasmid DNA (100 mg/mouse) of pcDNA3.1-T289 (expressing human TSHR A subunit cDNA, NM_000369.2), pcDNA3.1(+), or saline as the mock control. Injections were immediately followed by electroporation with an ECM 830 system (BTX Harvard Apparatus) with 10 mm electrode needles at 200 V/cm. The current was applied in ten 20 ms square wave pulses at 1 Hz and caused marked muscle twitching. Injections were carried out four times over a 3-week period. Mice were monitored for signs of distress afterwards, including weight loss and behavior changes such as fur-ruffling and lethargy. 15 weeks after the last immunization, all mice were humanely euthanized and the orbital tissue was removed.

To test the role of TMEM2, mice were randomly assigned to three groups: control, GO, and GO + TMEM2. Overexpression of TMEM2 *in vivo* was facilitated by adeno-associated virus (AAV)-mediated delivery through tail vein injection (1×10^{11} v.g per mouse). A week later, mice were immunized to induce GO as described before.

Cell culture and differentiation protocol

Orbital tissue was removed from GO or non-GO mice, minced, and placed into plastic culture dishes in Medium 199 containing 20% fetal bovine serum (FBS; Gibco), penicillin (100 U/ml) and gentamicin (20 μg/ml) at 37 °C in a humidified atmosphere of 5% CO_2. Once OFs had grown out from the tissue extracts, the cells were passaged and cultured in media containing 10% FBS and antibiotics.

To initiate adipocyte differentiation, OFs were grown to confluence in six-well plates, then the media was replaced with serum-free DMEM-Ham's F-12 (1:1; Gibco) containing biotin (33 μmol/L), pantothenic acid (17 μmol/L), transferrin (10 μg/ml), T3 (0.2 nmol/L), insulin (1 μmol/L), carbaprostacyclin (cPGI2; 0.2 μmol/L), and, for the first 4 days, dexamethasone (1 μmol/L) and isobutylmethylxanthine (IBMX; 0.1 mmol/L). Cells were cultured under these differentiation conditions for 10 days and the media was replaced every 3 to 4 days.

RNA extraction and qPCR

Total RNA was extracted, and reverse transcribed into cDNA using the HiScript Reverse Transcriptase (RNase H) (Vazyme). The cDNA was amplified using SYBR Green Real-Time PCR master mix and a StepOne Plus real-time PCR thermocycler (Applied Biosystems). The following PCR primer sequences were used: TMEM2, forward: 5′-ATATGGGCCGGTATCCT GTG-3′ and reverse: 5′-ACCTAGTGTGTCGAAGCCAA-3′; and GAPDH, forward: 5′-ATGGGTGTGAACCACGAGA-3′ and reverse: 5′- CAGGGATGATGTTCTGGGCA-3′. All PCR reactions were performed in triplicate. Samples were normalized to GAPDH levels and are expressed as the relative fold change of threshold cycle value relative to the control group using the $2^{-\Delta\Delta Ct}$ method.

Construction of TMEM2 overexpression and silencing vectors and transfections

TMEM2 overexpression vector was constructed by inserting the TMEM2 coding sequence into the pcDNA3.1+ vector. For shRNA-mediated silencing of TMEM2, the shRNA sequence (shTMEM2: GTGAGAAACTATGAAAATCATAG) was cloned into the pLKO.1 vector (Genepharm).

For overexpression studies, OFs were grown to 70 to 90% confluency and transfected with the TMEM2 overexpression vector using Lipofectamine 3000 reagent (Thermo Fisher Scientific) for 48 h. For the knockdown experiments, OFs were cultured to 80% confluency and transfected with scramble shRNA or shTMEM2 using the Lipofectamine 3000 reagent for 48 h. Following transfection, cells were treated with IL-1β (10 ng/ml) to induce inflammation or H_2O_2 (200 μM) to induce oxidative stress. Transfected cells were differentiated into adipocytes for 10 days to determine the effects of TMEM2 knockdown on adipogenesis.

Enzyme-linked immunosorbent assay (ELISA)

ELISA was used to determine the IL-6 and IL-8 levels released by OFs. Briefly, the culture medium of treated cells was collected and centrifuged at 2000*g* for 10 min. The resulting supernatant was assayed immediately using IL-6 and IL-8 ELISA kits according to the manufacturer's instructions (R&D). The absorbance was read at 450 nm using a spectrophotometer (Rayto RT-6100).

Oil red O staining

OFs cultured under adipogenic conditions as described above were washed twice with PBS, then fixed with 3.7% formalin for 1 h at 4 °C. Fixed samples were stained with oil-red O working solution for 1 h at room temperature. After washing in distilled water, samples were visualized, and images were captured by light microscopy. Lipid accumulation was assessed by solubilizing cell-bound oil red O with 100% isopropanol and measuring the optical density of the solution with a spectrophotometer at 490 nm.

Measurement of reactive oxygen species (ROS) levels

ROS levels were measured using the cell-permeant 5(6)-carboxy-2′,7′-dichlorofluorescein diacetateoxidant-sensitive fluorescent probe (H2DCFDA; Sigma-Aldrich). Briefly, OFs were seeded in 24-well plates at a density of 1×10^5 cells/ml. Cells were transfected with TMEM2 overexpression vector or shTMEM2 and their corresponding empty vector and scramble shRNA controls for 48 h as described above. Next, cells were treated with H_2O_2 (200 μM) for 1 h to induce oxidative stress or IL-1β (10 ng/ml) for 24 h to induce inflammation. Treated cells were then washed with PBS and incubated with H2DCFDA (10 μM) at 37 °C. Samples were trypsinized, washed, resuspended in PBS, and examined by flow cytometry (Nikon Eclipse C1).

Western blot analysis

OFs were lysed on ice for 30 min in cell lysis buffer containing HEPES (20 mM, pH 7.2), 10% glycerol, Na_3VO_4 (10 mM), NaF (50 mM), PMSF (1 mM), DTT (0.1 mM), leupeptin (1 μg/ml), pepstatin (1 μg/ml), and 1% Triton X-100. Protein concentrations were determined using the Bradford assay (Bio-Rad). Equal amounts of protein were separated by 10% SDS-PAGE, then transferred to PVDF membranes. Membranes were blocked with skimmed milk, then incubated overnight with primary antibodies against TMEM2 (1:1000; Proteintech), adiponectin (1:500; Abcam), PPAR-γ (1:1000; Abcam), c/EBPα (1:500; Abcam), c/EBPβ (1:1000; Abcam), p-Tyk2 (1:1000; Sigma-Aldrich), Tyk2 (1:1000; Sigma-Aldrich),p-JAK1 (1:1000; Cell Signaling Technology), JAK1 (1:1000; Cell Signaling Technology, Danvers, MA), p-Stat1 (1:1000; Abcam), Stat-1 (1:1000; Abcam), p-Stat2 (1:1000; Sigma-Aldrich), Stat-2 (1:1000; Sigma-Aldrich) and GAPDH (1:2000; Cell Signaling Technology). After washing with TBST three times, membranes were incubated with horseradish peroxidase (HRP)-conjugated secondary antibodies for 1 h at room temperature. After a further three washes with TBST, protein bands were visualized using an enhanced chemiluminescence kit (Pierce). The relative amount of each immunoreactive band was quantified by densitometry and normalized to GAPDH.

Immunohistochemistry (IHC)

Orbital tissue sections from GO and non-GO mice were fixed in formalin and embedded in paraffin. Antigen retrieval was carried out by microwaving the tissue samples in citrate buffer. Sections were then incubated in H_2O_2 (10 μg/ml) for 20 min to inhibit endogenous peroxidase activity. Next, sections were washed in PBS for 10 min, blocked with 3% BSA for 30 min at room temperature, and then incubated with a primary antibody against TMEM2 (1:100; Proteintech) for 12 h at 4 °C. Sections were then washed in PBS and incubated with the HRP-conjugated secondary antibody for 1 h at room temperature. Samples were washed with PBS, then developed using 3-3′ diaminobenzidine tetrahydrochloride (DAB; Sigma). Sections were counterstained with Mayer's hematoxylin, washed and mounted. Stained samples were visualized by light microscopy.

Immunofluorescence assay

In order to determine CD3 expression in orbital tissues, immunofluorescence staining was performed. The OFs were fixed in 10% neutral buffered formalin and permeabilized by 0.3% Triton X-100 in PBS. Fixed tissue or cells were rinsed in PBS, incubated in blocking solution (1% BSA, 0.3% Triton X-100 in PBS) for 30 min, then incubated in CD3 antibody (1:10; Abcam) solution at 4 °C overnight. The tissue or cells were washed three times in PBS and incubated in Alexa-488-conjugated secondary antibody (Invitrogen) for 1 h at room temperature. Finally, the tissue or cells were rinsed twice in PBS, and counterstained with DAPI for 5 min, and images were taken by fluorescence microscope (Olympus).

Nile red staining

Cultured OFs were rinsed with 0.1 mol/L PBS and fixed with 2% PBS-buffered formaldehyde containing 0.2% Triton X-100 and 5% sucrose at 37 °C for 5 min. After a thorough PBS rinse (three times, 5 min each), the cells were further permeabilized with 60% isopropanol solution in PBS (5 min) and incubated with 1:100 buffer diluted Nile red stock solution (Invitrogen) for 5 min. Cultures were washed in PBS three times and the coverslips inverted and finally mounted on object slides with ProLong Glass Mountant (Invitrogen).

To evaluate the presence of lipids in orbital tissue, the deparaffinized orbital tissue sections were hydrated in graded ethanol for 5 min each. After washing in PBS, the sections were stained by using Nile Red (0.5 μl/ml) at room temperature for 1 h. Samples were analyzed by using a fluorescent microscope.

Hematoxylin and eosin (H&E) and Masson's trichrome staining

Orbital tissue from GO and non-GO mice was fixed in neutral formalin, embedded in paraffin, then sectioned. The slides were subjected to H&E or Masson's trichrome staining. Samples were visualized and images were captured by light microscopy.

Statistical analysis

All experiments were performed at least three times and samples were assayed in duplicate each time. For statistical analysis of qPCR and Western blot assays, the mean value and SD were calculated for normalized measurements of each

ASBMB

mRNA or protein from multiple samples harvested from different treatment groups. Data were analyzed by the t test or one-way ANOVA test and Bonferroni method as a post hoc test using the GraphPad 8.0 program for Windows. A p value < 0.05 was considered significant.

Ethics approval

All procedures involving animals were in compliance with the National Institutes of Health guide for the care and use of Laboratory animals, and ethical approval was granted by the Shanghai University of Traditional Chinese Medicine Ethics Committee. All experiments were performed in accordance with relevant guidelines and regulations.

Data availability

All supporting data are included within the main article.

Author contributions—L. H., M. J. conceptualization, L. H. resources, L. H., M. J. writing–review & editing, L. H. supervision, L. H. project administration, L. H. funding acquisition; M. J. methodology; M. J., S. W. validation; M. J., Y. Y., and T. J. investigation; M. J. writing–original draft; W. W.: Software; Q. Y. data curation.

Funding and additional information—The research leading to these results received funding from The National Natural Science Foundation of China, Grant/Award Number:81373617, 81072793 and 30772800; Shanghai Committee of Science and Technology Research Projects, Grant/Award Number: 19140904600, 18401900800 and 15401930400; Shanghai Municipal Health Commission Research Projects, Grant/Award Number: 2020JQ001.

Conflict of interest—The authors have no conflicts of interest to declare that are relevant to the content of this article.

Abbreviations—The abbreviations used are: FBS, fetal bovine serum; GO, Graves' orbital; GSEA, Gene set enrichment analysis; HA, Hyaluronic acid; H&E, Hematoxylin and eosin; hTSHR, human TSH receptor; JAK, Janus kinase; OFs, Orbital fibroblasts; STAT, signal transducer and activator of transcription; TMEM2, transmembrane protein 2.

References

1. Taylor, P. N., Zhang, L., Lee, R. W. J., Muller, I., Ezra, D. G., Dayan, C. M., *et al.* (2020) New insights into the pathogenesis and nonsurgical management of Graves orbitopathy. *Nat. Rev. Endocrinol.* **16**, 104–116
2. Yoon, J. S., and Kikkawa, D. O. (2022) Thyroid eye disease: from pathogenesis to targeted therapies. *Taiwan J. Ophthalmol.* **12**, 3–11
3. Longo, C. M., and Higgins, P. J. (2019) Molecular biomarkers of Graves' ophthalmopathy. *Exp. Mol. Pathol.* **106**, 1–6
4. Huang, Y., Fang, S., Li, D., Zhou, H., Li, B., and Fan, X. (2019) The involvement of T cell pathogenesis in thyroid-associated ophthalmopathy. *Eye (Lond)* **33**, 176–182
5. Garantziotis, S., and Savani, R. C. (2019) Hyaluronan biology: a complex balancing act of structure, function, location and context. *Matrix Biol.* **78-79**, 1–10
6. Litwiniuk, M., Krejner, A., Speyrer, M. S., Gauto, A. R., and Grzela, T. (2016) Hyaluronic acid in inflammation and tissue regeneration. *Wounds* **28**, 78–88
7. Wong, Y. K., Tang, K. T., Wu, J. C., Hwang, J. J., and Wang, H. S. (2001) Stimulation of hyaluronan synthesis by interleukin-1beta involves activation of protein kinase C betaII in fibroblasts from patients with Graves' ophthalmopathy. *J. Cell Biochem.* **82**, 58–67
8. Yoon, Y., Chae, M. K., Lee, E. J., and Yoon, J. S. (2020) 4-Methylumbelliferone suppresses hyaluronan and adipogenesis in primary cultured orbital fibroblasts from Graves' orbitopathy. *Graefes Arch. Clin. Exp. Ophthalmol.* **258**, 1095–1102
9. Scott, J. E. (1992) Supramolecular organization of extracellular matrix glycosaminoglycans, *in vitro* and in the tissues. *FASEB J.* **6**, 2639–2645
10. Dokoshi, T., Zhang, L. J., Nakatsuji, T., Adase, C. A., Sanford, J. A., Paladini, R. D., *et al.* (2018) Hyaluronidase inhibits reactive adipogenesis and inflammation of colon and skin. *JCI Insight* **3**, e123072
11. Csoka, A. B., Frost, G. I., and Stern, R. (2001) The six hyaluronidase-like genes in the human and mouse genomes. *Matrix Biol.* **20**, 499–508
12. Stern, R. (2004) Hyaluronan catabolism: a new metabolic pathway. *Eur. J. Cell Biol.* **83**, 317–325
13. Irie, F., Tobisawa, Y., Murao, A., Yamamoto, H., Ohyama, C., and Yamaguchi, Y. (2021) The cell surface hyaluronidase TMEM2 regulates cell adhesion and migration *via* degradation of hyaluronan at focal adhesion sites. *J. Biol. Chem.* **296**, 100481
14. Tobisawa, Y., Fujita, N., Yamamoto, H., Ohyama, C., Irie, F., and Yamaguchi, Y. (2021) The cell surface hyaluronidase TMEM2 is essential for systemic hyaluronan catabolism and turnover. *J. Biol. Chem.* **297**, 101281
15. Yamamoto, H., Tobisawa, Y., Inubushi, T., Irie, F., Ohyama, C., and Yamaguchi, Y. (2017) A mammalian homolog of the zebrafish transmembrane protein 2 (TMEM2) is the long-sought-after cell-surface hyaluronidase. *J. Biol. Chem.* **292**, 7304–7313
16. Kudo, Y., Sato, N., Adachi, Y., Amaike, T., Koga, A., Kohi, S., *et al.* (2020) Overexpression of transmembrane protein 2 (TMEM2), a novel hyaluronidase, predicts poor prognosis in pancreatic ductal adenocarcinoma. *Pancreatology* **20**, 1479–1485
17. Lee, H., Goodarzi, H., Tavazoie, S. F., and Alarcon, C. R. (2016) TMEM2 is a SOX4-regulated gene that mediates metastatic migration and invasion in breast cancer. *Cancer Res.* **76**, 4994–5005
18. Yoneyama, M. S., Yoneyama, T., Tobisawa, Y., Yamamoto, H., Hatakeyama, S., Yoneyama, T., *et al.* (2022) TMEM2 expression is downregulated as bladder cancer invades the muscle layer. *Biochem. Biophys. Res. Commun.* **613**, 1–6
19. Schinzel, R. T., Higuchi-Sanabria, R., Shalem, O., Moehle, E. A., Webster, B. M., Joe, L., *et al.* (2019) The hyaluronidase, TMEM2, promotes ER homeostasis and longevity independent of the UPR(ER). *Cell* **179**, 1306–1318.e18
20. Zhu, X., Xie, C., Li, Y. M., Huang, Z. L., Zhao, Q. Y., Hu, Z. X., *et al.* (2016) TMEM2 inhibits hepatitis B virus infection in HepG2 and HepG2.2.15 cells by activating the JAK-STAT signaling pathway. *Cell Death Dis.* **7**, e2239
21. Xia, N., Ye, X., Hu, X., Song, S., Xu, H., Niu, M., *et al.* (2017) Simultaneous induction of Graves' hyperthyroidism and Graves' ophthalmopathy by TSHR genetic immunization in BALB/c mice. *PLoS One* **12**, e0174260
22. Angell, H. K., Lee, J., Kim, K. M., Kim, K., Kim, S. T., Park, S. H., *et al.* (2019) PD-L1 and immune infiltrates are differentially expressed in distinct subgroups of gastric cancer. *Oncoimmunology* **8**, e1544442
23. Kim, S. E., Lee, J. H., Chae, M. K., Lee, E. J., and Yoon, J. S. (2016) The role of Sphingosine-1-phosphate in adipogenesis of Graves' orbitopathy. *Invest. Ophthalmol. Vis. Sci.* **57**, 301–311
24. Achari, A. E., and Jain, S. K. (2017) Adiponectin, a therapeutic target for obesity, diabetes, and endothelial dysfunction. *Int. J. Mol. Sci.* **18**, 1321
25. Stewart, C. E., Randall, R. E., and Adamson, C. S. (2014) Inhibitors of the interferon response enhance virus replication *in vitro*. *PLoS One* **9**, e112014
26. Dik, W. A., Virakul, S., and van Steensel, L. (2016) Current perspectives on the role of orbital fibroblasts in the pathogenesis of Graves' ophthalmopathy. *Exp. Eye Res.* **142**, 83–91
27. Moshkelgosha, S., So, P. W., Deasy, N., Diaz-Cano, S., and Banga, J. P. (2013) Cutting edge: retrobulbar inflammation, adipogenesis, and acute orbital congestion in a preclinical female mouse model of Graves' orbitopathy induced by thyrotropin receptor plasmid-in vivo electroporation. *Endocrinology* **154**, 3008–3015

28. Draman, M. S., Zhang, L., Dayan, C., and Ludgate, M. (2021) Orbital signaling in Graves' orbitopathy. *Front. Endocrinol. (Lausanne)* **12**, 739994
29. Kaul, A., Short, W. D., Wang, X., and Keswani, S. G. (2021) Hyaluronidases in human diseases. *Int. J. Mol. Sci.* **22**, 3204
30. Galgoczi, E., Jeney, F., Katko, M., Erdei, A., Gazdag, A., Sira, L., *et al.* (2020) Characteristics of hyaluronan synthesis inhibition by 4-methylumbelliferone in orbital fibroblasts. *Invest. Ophthalmol. Vis. Sci.* **61**, 27
31. Zhang, L., Grennan-Jones, F., Draman, M. S., Lane, C., Morris, D., Dayan, C. M., *et al.* (2014) Possible targets for nonimmunosuppressive therapy of Graves' orbitopathy. *J. Clin. Endocrinol. Metab.* **99**, E1183–1190
32. Forrester, S. J., Kikuchi, D. S., Hernandes, M. S., Xu, Q., and Griendling, K. K. (2018) Reactive oxygen species in metabolic and inflammatory signaling. *Circ. Res.* **122**, 877–902
33. Kaneko, N., Kurata, M., Yamamoto, T., Morikawa, S., and Masumoto, J. (2019) The role of interleukin-1 in general pathology. *Inflamm. Regen.* **39**, 12
34. Zhou, H., Jia, X., Hu, K., Mo, Z., Xu, W., Peng, L., *et al.* (2021) TMEM2 binds to CSNK2A3 to inhibit HBV infection *via* activation of the JAK/STAT pathway. *Exp. Cell Res.* **400**, 112517
35. Byeon, H. J., Kim, J. Y., Ko, J., Lee, E. J., Don, K., and Yoon, J. S. (2020) Protein tyrosine phosphatase 1B as a therapeutic target for Graves' orbitopathy in an *in vitro* model. *PLoS One* **15**, e0237015
36. Tomer, Y., Ban, Y., Concepcion, E., Barbesino, G., Villanueva, R., Greenberg, D. A., *et al.* (2003) Common and unique susceptibility loci in Graves and Hashimoto diseases: results of whole-genome screening in a data set of 102 multiplex families. *Am. J. Hum. Genet.* **73**, 736–747